PCCP

PAPER

View Article Online
View Journal | View Issue

Cite this: *Phys. Chem. Chem. Phys.*, 2017, **19**, 7270

Stabilization of carbocations CH_3^+, $C_2H_5^+$, i-$C_3H_7^+$, *tert*-Bu^+, and *cyclo*-pentyl$^+$ in solid phases: experimental data *versus* calculations†

Evgenii S. Stoyanov*[ab] and Anton S. Nizovtsev[bc]

Received 6th October 2016,
Accepted 7th February 2017

DOI: 10.1039/c6cp06839a

rsc.li/pccp

Comparison of experimental infrared (IR) spectra of the simplest carbocations (with the weakest carborane counterions in terms of basicity, $CHB_{11}Hal_{11}^-$, Hal = F, Cl) with their calculated IR spectra revealed that they are completely inconsistent, as previously reported for the *t*-Bu^+ cation [Stoyanov E. S., *et al. J. Phys. Chem. A*, 2015, **119**, 8619]. This means that the generally accepted explanation of hyperconjugative stabilization of the carbocations should be revised. According to the theory, one CH bond (denoted as CH♣) from each CH_3/CH_2 group transfers its σ-electron density to the empty $2p_z$ orbital of the sp^2 C atom, whereas the σ-electron density on the other CH bonds of the CH_3/CH_2 group slightly increases. From experimental IR spectra it follows that donation of the σ-electrons from the CH♣ bond to the $2p_z$ C-orbital is accompanied by equal withdrawal of the electron density from other CH bonds, that is, the electrons are supplied from each CH bond of the CH_3/CH_2 group. As a result, all CH stretches of the group are red shifted, and IR spectra show typical CH_3/CH_2 group vibrations. Experimental findings provided another clue to the electron distribution in the hydrocarbon cations and showed that the standard computational techniques do not allow researchers to explain a number of recently established features of the molecular state of hydrocarbon cations.

Introduction

The research on carbocation stabilization is one of the most important trends in carbocation chemistry. Experimental studies mainly deal with gas phase infrared (IR) mass spectroscopy,[1–4] IR and NMR characterization in superacidic media,[5–12] and X-ray structural analysis.[13–17] As shown by *ab initio* calculations, the isolated carbocations are stabilized due to the intramolecular charge distribution under the influence of hyperconjugation[1,18–22] and polarization.[23] The simplest carbocation, CH_3^+, is subject to only the polarization effect.[23] For the gaseous $C_2H_5^+$ cation, the theory predicts and experiments confirm that the hyperconjugative interaction between the CH_3 group and the empty $2p_z$ orbital in the carbon atom of the CH_2 group is so strong that a bridged-proton symmetrical structure is formed.[3] The isolated i-propyl (i-Pr^+) cation has been the subject of extensive *ab initio* calculations.[24–27] In its lowest-energy C_2 conformer, two C–H bonds are aligned with the up and down lobes of the $2p_z$ orbital of the sp^2 C-atom, suggesting that these C–H bonds are involved in strong hyperconjugation.

Most attention has been given to the *tert*-butyl cation, whose hyperconjugative delocalization of the positive charge has been used as a textbook explanation of its stability. As predicted by quantum chemical calculations, the most energetically stable *t*-Bu^+ cation (C_s symmetry) has three CH bonds, one from each CH_3 group, which are aligned in parallel with the empty $2p_z$ orbital of the central sp^2 carbon atom.[1,18–20] This situation makes donation of its σ-electron density to this orbital possible, resulting in σ-p_z hyperconjugation (Scheme 1). These three C–H bonds (one of them is marked with ♣ in Scheme 1) are weakened and their νCH frequencies are significantly decreased, whereas the remaining C–H bonds (CH′ and CH″ in Scheme 1) are slightly strengthened and their νCH increases.

Thus, *ab initio* calculations predict a coherent picture of the mechanism underlying positive charge dispersion in the naked cations $C_2H_5^+$, $(CH_3)_2CH^+$ (i-Pr^+), and $(CH_3)_3C^+$ (*t*-Bu^+) primarily

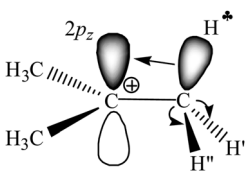

Scheme 1 Schematic representation of the electron density redistribution in accordance with the classical understanding of the mechanism of hyperconjugation stabilization in *t*-Bu^+.

[a] *Vorozhtsov Institute of Organic Chemistry, Siberian Branch of Russian Academy of Sciences, Novosibirsk 630090, Russia. E-mail: evgenii@nioch.nsc.ru*
[b] *Department of Natural Sciences, National Research University, Novosibirsk State University, Novosibirsk 630090, Russia*
[c] *Nikolaev Institute of Inorganic Chemistry, Siberian Branch of Russian Academy of Sciences, Novosibirsk 630090, Russia*

† Electronic supplementary information (ESI) available. See DOI: 10.1039/c6cp06839a

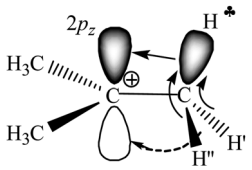

Scheme 2 Schematic representation of electron density redistribution in t-Bu$^+$ according to empirical data.[28]

via the hyperconjugative effect. It is clear that the polarization effect must play an important role in cation stabilization although convincing data based on calculations are actually absent.

Our recent experimental study of the t-Bu$^+$ cation in condensed phases, together with interpreted IR spectra of gaseous t-Bu$^+$, showed[28] that empirical findings contradict the generally accepted hyperconjugation mechanism (Scheme 1). It follows from the experiments that all C–H bonds of the two CH_3 groups of t-Bu$^+$ donate σ-electrons to the carbon's $2p_z$ orbital (Scheme 2), and the third CH_3 group is mostly affected by polarization.

It should be noted that in condensed phases, there is an additional intermolecular effect of carbocation stabilization: hydrogen bonding with the immediate surroundings. It leads to the strengthening of hyperconjugation and contributes to the scattering of the positive charge to the environment.[17,28]

In the present work we expanded the comparison of the computational results explaining stabilization of carbocations (structurally optimized and having the lowest energy) with empirical findings in IR spectra of carbocations in the series CH_3^+, $C_2H_5^+$, i-$C_3H_7^+$, t-Bu$^+$, and *cyclo*-$C_5H_9^+$, with the carborane counterions ($CHB_{11}Hal_{11}^-$, Hal = F, Cl; hereinafter abbreviated as $\{Hal_{11}^-\}$, see Fig. 1), whose conjugated acids are the strongest pure Brønsted superacids available today.[29,30] We established that IR spectra of $\{F_{11}^-\}$ or $\{Cl_{11}^-\}$ in ionic carbocation salts are not dependent on the nature of the cation and therefore are not considered here. The aims of the present study were (i) to determine whether t-Bu$^+$ is a special case of a cation or a common representative of saturated carbocations and (ii) to verify the compatibility of the theoretical data with experimental results for a range of simplest carbocations. We focused on the C–H stretch vibrations because they are mostly sensitive to hyperconjugation and polarization effects. Despite the importance of intermolecular hydrogen bonding for carbocation stabilization in the condensed phase, this effect will not be examined here in detail because it does not change the hyperconjugation mechanism when going from vacuum to a condensed phase as shown previously.[17,28]

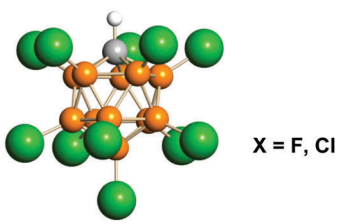

Fig. 1 Icosahedral carborane anions of $CHB_{11}Hal_{11}^-$ type (Hal = F, Cl) abbreviated as $\{F_{11}^-\}$ or $\{Cl_{11}^-\}$. Halogen atoms are depicted in green.

Experimental

All sample handling was carried out in an inert atmosphere (H_2O, O_2 < 1 ppm) in a dry box. Carborane acids H$\{Hal_{11}\}$ and their $CH_3\{Hal_{11}\}$ salts were prepared as previously described.[30–33] The salts of $C_2H_5^+$ and $C_3H_7^+$ cations with the $\{F_{11}^-\}$ anion were obtained by reacting CH_3F with H$\{F_{11}\}$ in an IR cell-reactor with simultaneous recording of the IR spectra of the formed cations.[33]

The spectrum of the $C_3H_7^+\{F_{11}^-\}$ salt was also obtained in another way: instead of the H$\{F_{11}\}$ acid, $Et_3Si\{F_{11}\}$ was used, synthesized as described in ref. 30. A small drop of liquid 2-Cl-propane was added to an excess of solid $Et_3Si\{F_{11}\}$ placed on the surface of the diamond attenuated total reflectance (ATR) accessory. A rapid reaction takes place

$$Et_3Si\{F_{11}\} + C_3H_7Cl \rightarrow C_3H_7^+\{F_{11}^-\} + Et_3SiCl\uparrow, \quad (1)$$

and gaseous Et_3SiCl is quickly removed. An ATR spectrum of the formed solid revealed strong absorption of the i-$C_3H_7^+\{F_{11}^-\}$ salt and weak absorption of unreacted (excess) $Et_3Si\{F_{11}\}$. Computer subtraction of the weak spectrum of residual $Et_3Si\{F_{11}\}$ allowed us to obtain a high quality spectrum of the i-$C_3H_7^+\{F_{11}^-\}$ salt.

The *cyclo*-$C_5H_9^+\{F_{11}^-\}$ salt was obtained by means of direct interaction of liquid *cyclo*-pentane with a powder of H$\{F_{11}\}$ in accordance with eqn (2):

$$cyclo\text{-}C_5H_{10} + H\{F_{11}\} \rightarrow C_5H_9^+\{F_{11}^-\} + H_2 \quad (2)$$

It was reported[30] that all alkanes, C_nH_m ($n \geq 4$), react with the H$\{F_{11}\}$ acid in the same way. Reaction (2) proceeded under ambient conditions for 4 hours. A white powder of the $C_5H_9^+\{F_{11}^-\}$ salt was obtained from the solution after vacuum removal of the solvent, *cyclo*-pentane.

IR spectra of isopropyl and *cyclo*-pentyl carbocations with the $\{Cl_{11}^-\}$ counterion were obtained as follows. A grain of the H$\{Cl_{11}\}$ acid was placed on the top face of the diamond crystal of the attenuated total reflectance (ATR) IR accessory and was wetted with a small drop of liquid 2-chloropropane or chloro-*cyclo*-pentane; this amount was not sufficient for full acid utilization. This approach ensures stoppage of the reaction at the first-stage, as illustrated in eqn (3) (an example of preparation of the i-Pr$^+$ salt):

$$C_3H_7Cl + H\{Cl_{11}\} \rightarrow C_3H_7^+\{Cl_{11}^-\} + HCl. \quad (3)$$

Recording the spectrum without applied pressure allowed us to obtain the spectrum of the oily byproduct covering the diamond surface as a thin film. This byproduct is formed when an excess of the chlorine hydrocarbon interacts with an acid. Recording the spectrum of the solid particles crushed under pressure, which contained mainly the carbocation salt and an excess of unreacted acid, enabled us to obtain their spectra with a minor overlap with the spectrum of byproducts. Computer-based subtraction of the spectrum of the byproducts and excess acid allowed for isolation of the carbocation spectra.

IR spectra were recorded on a Perkin Elmer Spectrum-100 spectrometer in the 4000–400 cm^{-1} frequency range in transmission or ATR mode. The spectrometer was installed inside

the dry box. The spectra were manipulated using GRAMMS/A1 (7.00) software from Thermo Scientific.

Computational details

Geometric parameters of the species under study were optimized at the B3LYP-D3/def2-TZVPD level of theory[34–37] using ultrafine grids. Equilibrium structures of compounds R{F_{11}} and *t*-Bu{Cl_{11}} were also calculated in a dichloroethane (DCE) solution (ε = 10.125) using the SMD solvation model.[38] All stationary points were characterized as minima by a vibrational analysis (the number of imaginary frequencies [NImag] was equal to zero), unless stated otherwise. Zero-point energies (ZPEs) were computed from the corresponding vibrational frequencies without scaling factors. (SMD-)B3LYP-D3/def2-TZVPD optimized structures were used in all subsequent computations.

To compare calculated and experimental vibrational frequencies, (SMD-)B3LYP-D3/def2-TZVPD harmonic frequencies were scaled by a factor of 0.9674 as recommended by Kesharwani *et al.*[39] To obtain more accurate relative energies of some isomers, single-point high-level CCSD(T)/def2-TZVPD coupled-cluster computations[40] within a frozen core approximation were additionally performed.

The energy decomposition analysis (EDA)[41] was carried out for the most stable compounds at the B3LYP-D3/TZ2P level of theory using the scalar relativistic (SR) zeroth-order regular approximation (ZORA) Hamiltonian (core potentials were not used, and the quality of the Becke numerical integration grid was set to the keyword good).[42]

SR-ZORA-B3LYP-D3/TZ2P computations were performed using the ADF2016 software,[43–45] while the remaining gas-phase calculations in the gas phase and in a DCE solution were conducted using the Gaussian09 software.[46] The natural bond orbital (NBO) analysis[47,48] was performed for the species of interest as implemented in Gaussian09. def2-TZVPD basis sets were taken from the EMSL database.[49,50]

Density functional theory (DFT) calculations with periodic boundary conditions were performed using the PBE functional[51] with D3 dispersion correction[36] using the VASP software package.[52,53] The projector augmented wave (PAW) method[54] was used to analyze the core states along with a plane-wave energy cutoff of 400 eV. Only the Γ point was used for sampling the Brillouin zone.

The convergence criteria for electronic and structural optimization were set to 10^{-6} eV and 10^{-5} eV Å^{-1}, respectively. Harmonic vibrational frequencies were calculated by the finite difference method using the central difference with a step size of 0.015 Å.

All compounds were considered in their ground states. The spin-restricted formalism was employed for both DFT and CCSD(T) computations.

Results and discussion

Characterization of carbocations on the basis of calculations

To obtain a unified computational view, we considered all carbocations (R^+) under study and their complexes with Ar and {F_{11}^-} in the gas phase and in solution at the same level of theory. The lowest-energy structures were chosen for subsequent analysis (see Fig. S1–S4 in ESI† for a complete list of isomers). The results obtained for the R^+, $R^+\cdots$Ar and R{F_{11}} species are given in Tables S1–S5 in ESI.† The stretching vibrations and some valent angles for naked and solvated carbocations are compared in Table 1.

The hyperconjugation effect is assumed to be the case starting from naked $C_2H_5^+$. In this cation, the hyperconjugation strength is so significant that the H^* proton is converted to the bridge state leading to a symmetrical structure[3] (II.1 in Fig. S1 in ESI†), which does exist in the condensed phase. Thus, we excluded the bridged structure from further analyses.

The $C_2H_5^+$ structure becomes asymmetrical after solvation by the Ar atom *via* the C center. The CH^* bond is oriented strictly parallel to the $2p_z$ orbital of the sp^2 C atom (θ = 0, see Scheme 3) and the $C–C–H^*$ angle is reduced (92.6°, Table 1); these data indicate a strong hyperconjugative interaction. The similar orientation of the CH^* bond from each CH_3 group relative to the $2p_z$ orbital of the sp^2 C atom has only naked *t*-Bu^+ (C_s, θ = 2°) and *t*-$Bu^+\cdots$Ar solvate (C_1, θ = 1°).This finding corresponds to the generally accepted mechanism of carbocation hyperconjugative stabilization (Scheme 1). Nevertheless, the θ angles of *t*-Bu^+ (C_1), despite almost the same relative energy as in *t*-Bu^+ (C_s), are increased by *ca.* 20°. The θ angle reaches values of 36° and 20° for the low-lying isomers of i-Pr^+ (C_{2v}) and i-$Pr^+\cdots$Ar (C_s) respectively (Fig. S2 and S3 in ESI†), which means that one C–H bond from each CH_3 group is perpendicular to the vacant $2p_z$ orbital, and two other C–H bonds are equivalently affected by hyperconjugation (Scheme 4). An intermediate case takes place in *c*-$C_5H_9^+$ and *c*-$C_5H_9^+\cdots$Ar species, with θ ranging from 12° to 13°. Thus, rotation of the CH_3 group by angle θ has a weak influence on the carbocation hyperconjugation stabilization.

The strong hyperconjugation influence on the CH_3 group in asymmetric $C_2H_5^+\cdots$Ar (Scheme 3) leads to a strong decrease in the CH^* stretch to 2612 cm^{-1}, whereas frequencies of the other two CH′ and CH″ bonds (νCH_2) are changed much less as compared to neutral hydrocarbons (Table 1). The νCH^* and νCH_2 frequencies are highly characteristic and are not mixed (Fig. S5b in ESI†). Unlike $C_2H_5^+$, solvation of other carbocations with Ar *via* the sp^2 C atom has a slight effect on the calculated IR spectra (Table 1). The spectra of all carbocations under study (both naked and solvated with Ar) show similar features: (i) the bands of C–H stretches affected by hyperconjugation are significantly red shifted and have increased intensity (bold faced in Table 1); (ii) frequencies of the other C–H bonds of CH_3/CH_2 groups are rather increased or are in the frequency region common for neutral hydrocarbons; (iii) the normal vibrations of these bonds or groups have a highly characteristic nature.

To gain insights into the bonding situation for the representative $R^+\cdots$Ar and R{F_{11}} complexes, we performed the EDA (Table S1 in ESI†) and NBO analyses (Table S2 in ESI†). The results of our gas-phase calculations for the carbocations paired with the {F_{11}^-} anion indicate the following: (a) in the case of R = C_2H_5, the hyperconjugation effect is the weakest one because of a covalent bond between ethyl and {F_{11}} leading to a modest energy gain corresponding to hyperconjugative stabilization ($\Delta E_{ij}^{(2)}$ = 9.2 kcal mol^{-1}; Table S2, ESI†) and rather weak IR intensity of

Table 1 CH stretch frequencies (scaled by a factor of 0.9674) and their IR intensities (km mol^{-1}, in parentheses) calculated at the B3LYP-D3/def2-TZVPD level of theory for the most energetically stable naked and Ar-solvated carbocations. Relevant structural parameters are also given

Compound	$C_2H_5^+\cdots$Ar	i-Pr$^+$		i-Pr$^+\cdots$Ar		*t*-Bu$^+$		*t*-Bu$^+\cdots$Ar		*c*-$C_5H_9^+$	*c*-$C_5H_9^+$Ar
Symmetry	C_s	C_2	C_{2v}	C_1	C_s	C_1	C_s	C_1	C_1	C_2	C_1
NImag	0	0	1	0	1	0	1	0	0	0	0
Relative energy,[a] kcal mol^{-1}	0	0	0.2	0	0.1	0	0	0	0.1	0	0
Dihedral angle θ, degrees[b]	0	17	36	13	20	21	2	1	14	13	12
C–C–H$^\clubsuit$ angle, degrees	92.6	102 102	107.8 107.8	101.4 102.8	104.6 104.6	104.9 105.9 106.8	103.3 104.1 104.1	103.2 104.1 104.1	103.9 104.3 105.2	98.1 98.1	98.1 98.6
Scaled CH stretches,[c] cm^{-1}	**2612** (154)	**2764** (224) **2777** (7)	**2841** (239) **2855** (1)	**2766** (145) **2799** (59)	**2803** (141) **2815** (54)	**2853** (91) **2864** (64) **2881** (34)	**2835** (109) **2838** (85) **2852** (19)	**2840** (78) **2843** (104) **2855** (9)	**2842** (93) **2851** (53) **2871** (33)	**2704** (130) **2712** (15)	**2711** (83) **2735** (45)
	2985 (17) 3024 (8) 3071 (11) 3128 (28)	2942 (54) 2944 (0) 3022 (0) 3053 (7) 3058 (9)	2856 (0) 2856 (64) 3022 (1) 3062 (9) 3068 (5)	2938 (28) 2960 (16) 3032 (0) 3053 (7) 3060 (8)	2921 (53) 2923 (11) 3032 (1) 3059 (8) 3067 (5)	2931 (16) 2944 (15) 2953 (10) 3050 (2) 3052 (3)	2974 (5) 2975 (2) 2977 (8) 3044 (3) 3046 (1)	2976 (3) 2977 (5) 2981 (5) 3045 (2) 3049 (2)	2952 (12) 2970 (8) 2972 (5) 3048 (2) 3049 (2)	2961 (0) 2969 (8) 2984 (22) 2986 (0) 3037 (0) 3042 (1)	2962 (0) 2970 (9) 2982 (12) 2994 (8) 3036 (1) 3042 (1)

[a] *E*(CCSD(T)/def2-TZVPD//B3LYP-D3/def2-TZVPD) + ZPE(B3LYP-D3/def2-TZVPD). [b] The θ angle is shown in Scheme 3. Averaged values of angle θ are presented. [c] The characteristic frequencies of C–H$^\clubsuit$ bonds mostly affected by hyperconjugation are boldfaced.

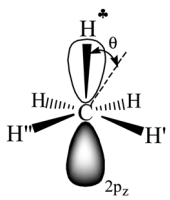

Scheme 3 A schematic representation of $C_2H_5^+$–Ar (C_{3v}, Ar is omitted) along the C–C bond. Dihedral angle θ shows deviation of the C–C–H$^\clubsuit$ plane from the direction of carbon's 2p$_z$ orbital.

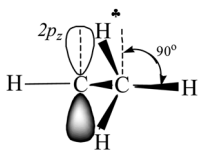

Scheme 4 Schematic representation of i-Pr$^+$ (C_{2v}). The views of the two CH_3 groups are overlapping.

the corresponding CH stretch vibration (Table S4, ESI†); (b) the spectrum of i-Pr$^+$ (Table S4 in ESI†) shows only some signs of weak hyperconjugation (two slightly decreased frequencies at 2923 and 2916 cm^{-1} with somewhat increased intensity), suggesting that the bonding between i-Pr and $\{F_{11}\}$ moieties is still covalent ($\Delta E_{ij}^{(2)}$ = 11.7 kcal mol^{-1}; Table S2, ESI†); (c) the spectra of *cyclo*-pentyl$^+$ and *t*-Bu$^+$ (Table S4 in ESI†) show greater resemblance to those of the corresponding Ar-solvated cations, as compared to the lighter carbocations.

NBO analysis revealed a polar covalent two-center two-electron C–F bond populated by 2.0 |e| at R = CH_3, C_2H_5, and i-Pr. Indeed, according to the EDA (Table S1 in ESI†), the electrostatic interaction (ΔE_{elstat}, 52–79%) between R^+ and $\{F_{11}^-\}$ moieties dominates over orbital (ΔE_{orb}) and dispersion (ΔE_{disp}) interactions in all compounds. On the other hand, the energy of orbital interactions makes a noticeable contribution to the total attractive interactions when R = CH_3 (47%), C_2H_5 (42%), and i-Pr (34%), in line with the calculated IR spectra. Thus, a covalent contribution to the C–F bond is present in all cases and gradually decreases in the order R = CH_3 < C_2H_5 < i-Pr < *cyclo*-pentyl ≤ *t*-Bu simultaneously with the increase of hyperconjugative stabilization in the same order as can be seen from the corresponding $\Delta E_{ij}^{(2)}$ values (Table S2, ESI†).

However, as will be illustrated below, all solid R$\{F_{11}\}$ compounds, except for $CH_3\{F_{11}\}$, are characterized by ionic bonding. The reason is the bulk effect, which most clearly manifests itself in the example of alkali halides. They are ionic in the solid state, but their neutral diatomics are linked covalently in the gas phase showing stretch vibration (for example, νNa–Cl at 364.6 cm^{-1}).[55] So, the crystal lattice promotes ionic binding.

To model the effect of the environment taking place in the condensed phase, we performed NBO and EDA analyses of the R$\{F_{11}\}$ species when they are transferred from the gas phase to a DCE solution. This change of the phase is accompanied by an increase of the R–$\{F_{11}\}$ distance (Tables S1 and S2, ESI†), which is relatively small for R = CH_3 (Δr = 0.033 Å) and pronounced when R = C_2H_5 (Δr = 0.120 Å), making the C–F bond more polar but retaining its covalent nature (ΔE_{orb}, 38–48%). In the case of i-$C_3H_7\{F_{11}\}$, the lengthening of C–F is the most pronounced (Δr = 0.604 Å), indicating that the character of the bond changes to presumably ionic (ΔE_{orb}, 16%; ΔE_{elstat}, 78%). Replacing i-$C_3H_7^+$ with *c*-$C_5H_9^+$ further increased the C–F separation to 2.584 Å, increasing the ionicity of the bond (ΔE_{orb}, 12%). Finally, the *t*-$C_4H_9\{F_{11}\}$ compound has the C–F distance typical for ionic species (>2.6 Å, ΔE_{orb}, 11%; Table S4, ESI†). Similar results were obtained in SMD-B3LYP-D3/def2-TZVPD calculations for

DCE solutions: the dielectric medium increased the separation between R and $\{Hal_{11}\}$ fragments (Fig. S4, ESI†), which made C–Hal bonds more ionic. The C–Cl distance in *t*-Bu$\{Cl_{11}\}$ became very close to that in an ionic salt (3.545 Å, Fig. S6, ESI†), resulting in a small covalent contribution—to the bonding between the ions (ΔE_{orb}, 14%; Table S1, ESI†)—approaching that in the solid phase. The calculated CH stretch frequencies for both phases also correlate well (Table S5, ESI†).

Increasing the ionicity of the R$\{F_{11}\}$ compounds in the series R = C_2H_5 < i-Pr < *cyclo*-pentyl < *t*-Bu strengthens the effect of hyperconjugation, as followed from the corresponding $\Delta E_{ij}^{(2)}$ values (Table S2, ESI†) and from the increase in the red-shift and intensity of the bands of CH stretches involved in hyperconjugation (Table S4, ESI†). It should be noted that the condensed phase enhances both ionicity and the effect of hyperconjugation in this series of R$\{F_{11}\}$ compounds gradually; this result contradicts experimental findings.

We have proved previously[56] that "effective" basicity of $\{F_{11}^-\}$ in the solid salt, $(HCO)^+\{F_{11}^-\}$, is close to the basicity of the Ar atom, and the calculated spectra of the Ar···H^+–CO and CO–H^+···Ar solvates agree well with the experimental spectra of ionic compound $(CO)H^+\{F_{11}^-\}$. Therefore, the experimental IR spectra of the ionic bulk salts under study are expected to better match the calculated IR spectra of weakly bound R^+–Ar solvates rather than R^+–$\{F_{11}^-\}$ species with a notable covalent contribution (Table S1 in ESI†). The same conclusion follows from DFT calculations for *t*-Bu$\{Cl_{11}\}$: the structure of *t*-Bu^+ in the *t*-Bu$\{Cl_{11}\}$ crystal (Fig. S7 in ESI†) is similar to that in the naked or Ar-solvated carbocation rather than to the structure of molecular compound *t*-Bu$\{Cl_{11}\}$ with a distorted *t*-Bu^+ moiety (Fig. S6a in ESI†). To sum up, computational results obtained for R^+–Ar (or naked R^+) should be used for comparison with the presented experimental findings.

Experimental IR spectra and properties of the carbocations

The CH_3^+ cation has an extremely high ability to bind to the bases. Even in the $CH_3\{F_{11}\}$ compound with the weakest basic ion $\{F_{11}^-\}$, the methyl group forms a highly polar covalent bond.[33]

The CH_3^+ cation is the most convenient object for evaluating the influence of the polarization effect on charge scattering over the methyl group in the absence of hyperconjugation.

Polarization is responsible for the transfer of some electron density from hydrogens to the central carbon. This effect leads to an increase of the CH stretch frequencies and strengthening of the force constants of CH bonds.[23,28,33] For methyl carboranes, $CH_3\{Hal_{11}\}$, the dependence of $\nu_{as}CH_3$ on anion basicity is linear and extrapolates to zero basicity (neat CH_3^+) at 3103 cm^{-1}.[33] This value corresponds to the true CH_3^+ cation in the condensed phase, and is very close to that obtained with the B3LYP-D3/def2-TZVPD approximation (3108 cm^{-1}, see Table S3 in ESI†).

$C_2H_5^+$ and i-$C_3H_7^+$ cations. An experimental IR spectrum of the $C_2H_5^+$ cation in vacuum, when targeted with Ar at H^+, shows three CH stretch vibrations (3114, 3032, and 2158 cm^{-1}) well-fitting those calculated for the non-classic bridged-proton symmetrical structure.[3] Thus, the hyperconjugative interaction in the bare cation is so strong that H^+ is equally shared between the two carbon atoms.

The IR spectrum of the ethyl carborane, $C_2H_5\{Cl_{11}\}$, revealed another extreme case:[32] all C–H stretch frequencies are in the region 2933–3057 cm^{-1} indicating covalent binding between C_2H_5 and $\{Cl_{11}\}$ moieties, which prevents the hyperconjugation effect. The frequencies of the CH_2 group of $C_2H_5\{Cl_{11}\}$ (3057 and 2976 cm^{-1}) are slightly higher than those of the chloronium cation $(C_2H_5)_2Cl^+$ (3038 and 2974 cm^{-1}), pointing to the more polar C–Cl bond in the case of $C_2H_5\{Cl_{11}\}$.

The $C_2H_5^+$ cation was obtained in the form of ionic salt $C_2H_5^+\{F_{11}^-\}$. Its formation through an unstable salt of fluoronium cation, $(CH_3)_2F^+$, is accompanied by the formation of i-Pr^+.[33] IR spectra showed the bands of both cations, whose intensities vary depending on the ratio of cations (Fig. 2a). Obtaining the difference between the spectra of the samples with a low and high portion of i-Pr^+ (Fig. 2, red and black)—up to full compensation of the absorption from i-$C_3H_7^+$—allowed us to obtain a spectrum of the $C_2H_5^+$ cation (Fig. 2b). Reverse subtraction of the spectra ("black" minus "red") did not fully remove the spectrum of the

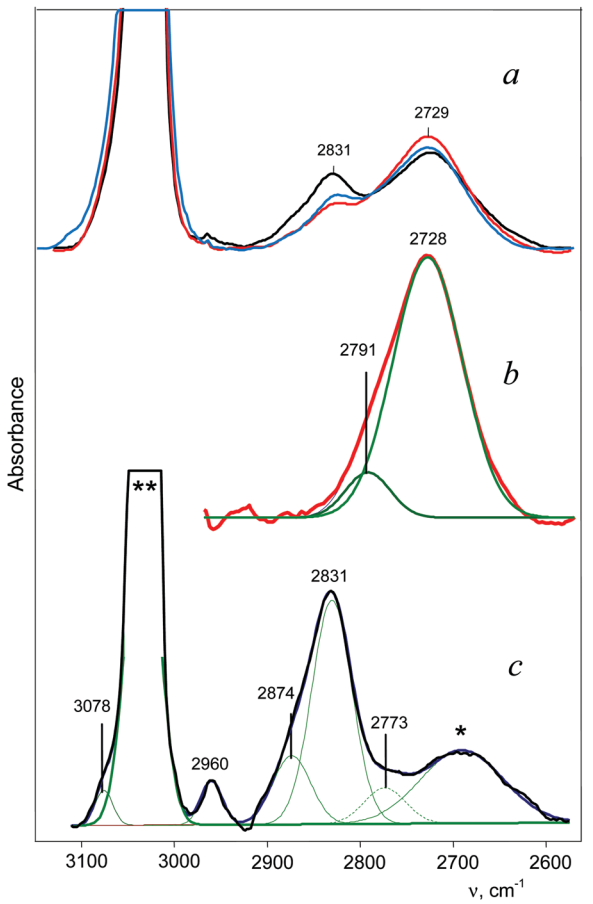

Fig. 2 IR spectra of (a) a mixture of $C_2H_5^+\{F_{11}^-\}$ and i-$Pr^+\{F_{11}^-\}$ salts,[33] showing the transformation of $C_2H_5^+$ into i-Pr^+ (red-blue-black); (b) the $C_2H_5^+$ cation spectrum obtained by subtracting the black spectrum (a) from the red spectrum (a) until full compensation of the band at 2831 cm^{-1} of i-Pr^+; (c) the i-$C_3H_7^+$ spectrum isolated by reverse subtraction of the spectra: black (a) minus red (a). An uncompensated remnant from $C_2H_5^+$ absorption is marked by an asterisk. The bands 3078 and 2960 cm^{-1} belong to the methyl group of the unreacted $CH_3\{F_{11}\}$ salt. The strong band, marked with **, belongs to the $\{F_{11}^-\}$ counterion.

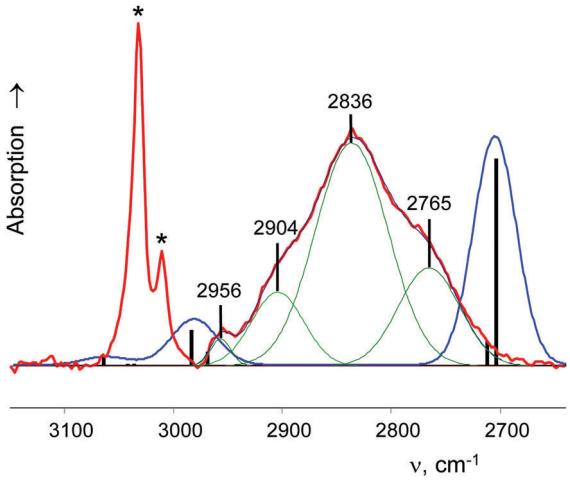

Fig. 3 The IR spectrum of the *cyclo*-$C_5H_9^+\{F_{11}^-\}$ salt (red; CH stretches of the anion are marked with asterisks) *versus* the calculated spectrum of naked *cyclo*-$C_5H_9^+$ at the B3LYP-D3/def2-TZVPD level of theory (blue curve; frequencies were scaled by a factor of 0.9674; band positions are indicated by black bars).

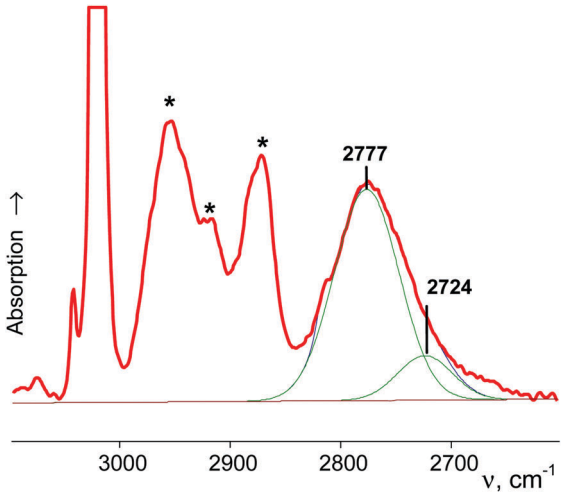

Fig. 4 The IR spectrum of *cyclo*-pentyl$^+\{Cl_{11}^-\}$, complicated by the bands of impurities from oligomeric cations (marked with asterisks).

$C_2H_5^+$ cation but allowed us to see the main features of the i-$C_3H_7^+$ spectrum (Fig. 2c). The absorption contour of CH stretches affected by hyperconjugation is asymmetric for both cations and can be broken down into at least two components (Fig. 2b and c).

The IR spectrum of the i-$C_3H_7^+\{F_{11}^-\}$ salt obtained in reaction (1) differs from the spectrum shown in Fig. 2c. This means that two isomers of i-$C_3H_7^+$ can form. This issue will be discussed below.

We did not succeed in obtaining a high-quality spectrum of the i-$C_3H_7^+\{Cl_{11}^-\}$ salt according to eqn (3) because formation of this salt is accompanied by formation of the chloronium cation $(C_3H_7)_2Cl^+$. Superimposition of the two spectra allowed us to determine only the maximum of the absorption from the C–H stretches of i-$C_3H_7^+$ disturbed by hyperconjugation (Fig. S8 in ESI†).

The *cyclo*-pentyl$^+$ cation. A white powder of the *cyclo*-$C_5H_9^+\{F_{11}^-\}$ salt obtained *via* direct interaction of acid $H\{F_{11}\}$ with *cyclo*-pentane (eqn (2)) yielded a high-quality IR spectrum (Fig. 3). Nevertheless, the *cyclo*-$C_5H_9^+\{Cl_{11}^-\}$ salt did not form in a similar manner. It was obtained in the reaction of $H\{Cl_{11}\}$ with chloro-*cyclo*-pentane; this reaction was accompanied by formation of oligomeric carbocations, which are degradation products of the intermediate chloronium cations decomposing at room temperature.[33] In Fig. 4, the IR bands from these byproducts are marked with asterisks. The important region of CH stretches of the *cyclo*-$C_5H_9^+$ cation, which was disturbed by hyperconjugation, was not distorted by impurities, and separation of their bands into individual components became possible.

The patterns observed in the IR spectra of the carbocations

t-Bu$^+$ is the most actively studied carbocation. On the basis of experimental data from the gaseous and condensed phase experiments, two CH_3 groups of the *t*-Bu$^+$ cation were proven to be involved in hyperconjugation.[28] All three CH bonds of each group donate σ-electrons to the $2p_z$ orbital of the sp^2 C atom (Scheme 2) and their CH stretches appear in IR spectra as group vibrations, ν_sCH_3 and $\nu_{as}CH_3$, with significantly decreased frequencies (at 2867, 2822 and 2771 cm^{-1} in the case of the salt with $\{F_{11}^-\}$ counterion, Fig. 5a). The third CH_3 group (marked as CH_3*) is predominantly polarized and shows three higher-frequency bands in the gas phase. This observation is supported by important experimental evidence: the stretch vibrations of CH_3 and CH_3* groups in *t*-Bu$^+$ show a good correlation (Table 2), which confirms their attribution to group vibrations and indicates that both types of CH_3 groups are isoelectronic.

Table 2 The valence group vibrations (in cm^{-1}) for gaseous *t*-Bu$^+$ with the proposed attribution

Group	$\nu_{as}CH_3$		ν_sCH_3
CH_3*	3038	2965	2913
CH_3	2880	2839	2793
Ratio	1.055	1.044	1.043

In addition, the C–H stretch frequencies of *t*-Bu$^+$ involved in hyperconjugation very well correlate with those of the isoelectronic planar trimethyl boron $(CH_3)_3B$[57] (Table 3). This observation confirms that the types of local CH_3 normal vibrations for both compounds coincide, and the electron distributions in their methyl groups are identical.

Finally, a good correlation was also observed between the frequencies of the CH_3* group in *t*-Bu$^+$ and those of the strongly polarized methyl group in $CH_3\{F_{11}\}$[33] (Table 4), confirming the above-mentioned conclusions.

In the condensed phases, *t*-Bu$^+$ forms noticeable H-bonds with the nearest surroundings favoring involvement of the CH_3* group in hyperconjugation, which is, however, weaker than that formed by its other two CH_3 groups.[28] This phenomenon is accompanied by enhanced dynamic properties of the H atoms of CH_3*, resulting in collapse of the three bands of CH_3* vibrations into one broad absorption (with an intensity of *ca.* 30% of that from all CH stretches) at a lower frequency[28] (Fig. 5a).

The spectrum of i-Pr$^+$ obtained in reaction (1) differs from that shown in Fig. 2b, but is very similar to the spectrum of *t*-Bu$^+$ (Fig. 5). It shows a broad absorption pattern at 2922 cm^{-1}

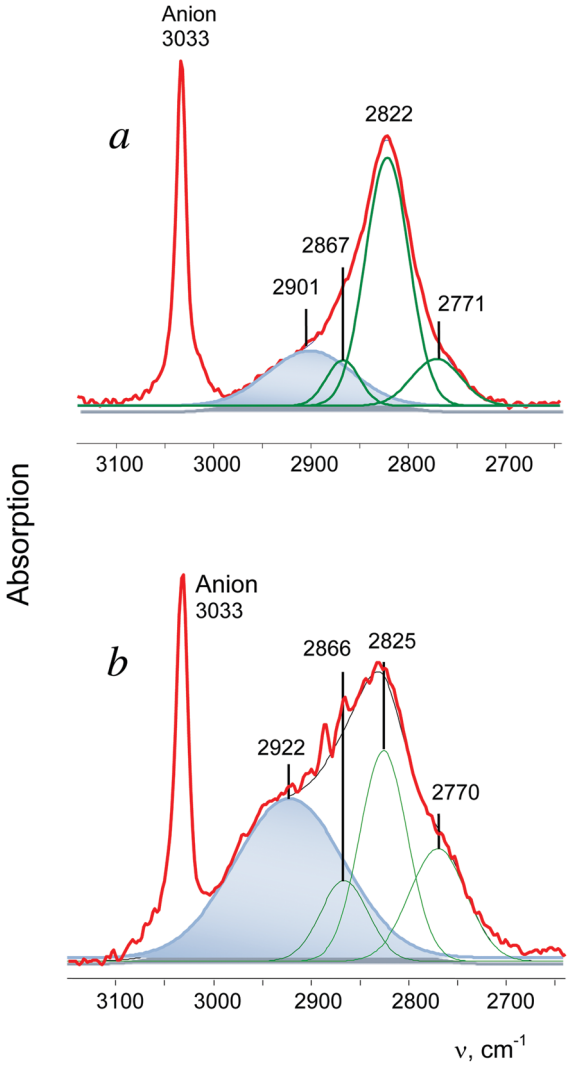

Fig. 5 IR spectra of cations *t*-Bu^+ (a) and i-$C_3H_7^+{}_{as}$ (b) in the salts with the $\{F_{11}^-\}$ anion. The spectra are broken down into Gaussian components. The broad absorption band is highlighted in blue. Compensation of the weak absorption of residual $Et_3Si\{F_{11}\}$, which was used in a small excess, leads to some remnants at 2900–2800 cm^{-1} that look like increased noise in spectrum (b).

Table 3 Comparison of experimental CH stretches of *t*-Bu^+ with those of isoelectronic $(CH_3)_3B$[57] (in cm^{-1})

Group	$\nu_{as}CH_3$		ν_sCH_3
t-Bu^+ gas	2880	2839	2793
$(CH_3)_3B$ gas	3000	2975	2875
Ratio	0.960	0.954	0.971

Table 4 Comparison of experimental CH stretches of the polarized CH_3* group of *t*-Bu^+ with those of the $CH_3\{F_{11}\}$ compound (in cm^{-1})

Group	$\nu_{as}CH_3$		ν_sCH_3
t-Bu^+ gas	3038	2965	2913
$CH_3\{F_{11}\}$ solid	3098	3086	2975
Ratio	0.981	0.961	0.979

with intensity *ca.* 50% of the total intensity of the CH stretch vibrations of i-Pr^+. The three bands at a lower frequency belong to the second CH_3 group involved in stronger hyperconjugation (the ratio of their intensity values may change, depending on the conditions of separation of the bands, but the number of bands is always three). Thus, the above-mentioned i-Pr^+ isomer is an analog of *t*-Bu^+, with similar asymmetry, and will be designated as i-Pr_{as}^+.

The spectrum of the second i-Pr^+ isomer contains only two bands of CH_3 groups involved in hyperconjugation (the third band was obviously not resolved) without the broad absorption (Fig. 2c). Thus, both CH_3 groups equally participate in hyperconjugation. Hereinafter, we will refer to this symmetrical isomer as i-Pr_{sym}^+.

The frequencies of hyperconjugated CH_3 groups for both i-Pr^+ isomers are close (Fig. 2c and 5b), which means that i-Pr_{as}^+ and i-Pr_{sym}^+ have roughly equal energy. Therefore, the efficiency of the positive charge redistribution over the CH_3 and CH_3* groups in carbocations is energetically equivalent.

A charged C_3 core of the *cyclo*-$C_5H_9^+$ cation is similar to that of i-Pr_{sym}^+. Its IR spectrum does not contain the broad absorption pattern (Fig. 3), indicating that this cation is symmetric. CH stretches of the two equivalent CH_2^α groups involved in hyperconjugation (Scheme 5) result in two low-frequency bands at 2836 and 2765 cm^{-1}. The remote CH_2^β groups yield the bands ν_{as} at 2956 and ν_s at 2904 cm^{-1}. Moreover, the ratio of frequencies for these bands coincides (Table 5). This finding implies identical assignment of frequencies for CH_2^α and CH_2^β groups and their isoelectronic character, as established for two types of CH_3 groups of *t*-Bu^+ (Table 2). This result leads to a major conclusion: both CH bonds of CH_2^α groups equally donate σ-electrons to the $2p_z$ orbital of the sp^2 C atom, in agreement with the case of *t*-Bu^+.

The $C_2H_5^+$ spectrum shows two bands from the CH_3 group vibrations, which are similar to those observed in the i-Pr_{sym}^+ spectrum (Fig. 2b and c). The broad absorption pattern, of course, is absent. This finding points to some generic relation between $C_2H_5^+$ and i-Pr_{sym}^+. The overall picture of the generic relations between the analyzed carbocations with hyperconjugative stabilization is shown in Fig. 6.

One can see that there are two kinds of carbocations: (i) carbocations with one type of hyperconjugated CH_3/CH_2 groups

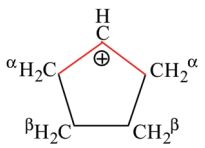

Scheme 5 Schematic representation of the *cyclo*-pentyl cation.

Table 5 CH stretch frequencies (in cm^{-1}) of the *cyclo*-pentyl cation

Group	$\nu_{as}CH_2$	ν_sCH_2
CH_2^α	2836	2765
CH_2^β	2956	2904
Ratio	0.959	0.952

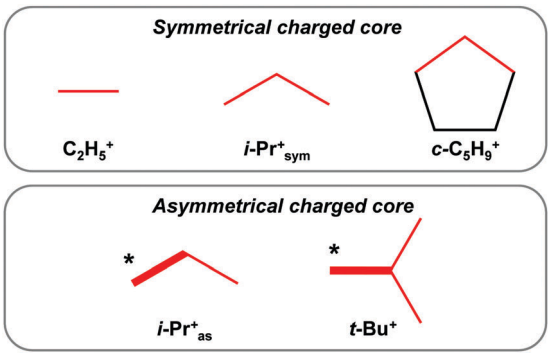

Fig. 6 The generic relation between the simplest carbocations with hyperconjugative stabilization. The charged core is marked in red; the C–C bond formed by the more strongly polarized CH_3* group is indicated by a bold red line.

Table 6 IR frequencies (in cm^{-1}) of the CH_3/CH_2 groups of carbocations under study affected by hyperconjugation

Cation	Anion	$\nu CH_3/\nu CH_2$		
$C_2H_5^+$	$\{F_{11}^-\}$	2791	**2728**[a]	
i-Pr_{sym}^+	$\{F_{11}^-\}$	2874	**2831**	
i-Pr_{as}^+	$\{F_{11}^-\}$	2866	**2825**	2770
t-Bu^+	$\{F_{11}^-\}$	2867	**2822**	2771
Cyclo-pentyl$^+$	$\{F_{11}^-\}$		**2836**	2765
i-Pr^+	$\{Cl_{11}^-\}$	[b]	**2780**	[b]
t-Bu^+ [28]	$\{Cl_{11}^-\}$	2830	**2791**	2746
Cyclo-pentyl$^+$	$\{Cl_{11}^-\}$		**2777**	2724

[a] The most intense bands are boldfaced. [b] Not determined.

($C_2H_5^+$, i-Pr_{sym}^+, and c-$C_5H_9^+$), which form a symmetrical C_3 charged core; (ii) carbocations with an asymmetrical C_3 or C_4 charged core formed by two types of CH_3 groups.

The frequencies of the CH_3/CH_2 groups mostly affected by hyperconjugation for all carbocations under study are summarized in Table 6. The decrease in the frequencies from $\{F_{11}^-\}$ to $\{Cl_{11}^-\}$ salts is due to the formation of H-bonds.[17]

All CH stretch vibrations of $C_2H_5^+$, i-Pr^+, *cyclo*-pentyl$^+$, and t-Bu^+ cations were observed in IR spectra with the exception of those from CH_2 and CH groups at the sp^2 C atom in $C_2H_5^+$ and i-Pr^+, respectively, which are weak and located in the frequency region of the intense C–H stretches from $\{F_{11}^-\}$ or $\{Cl_{11}^-\}$ anions.

Experimental data *versus* calculations. Experimental and calculated data showed that the impact of the environment on the nature of the R–$\{F_{11}\}$ bond may be significant. The CH_3 group is linked covalently to $\{F_{11}^-\}$, and the calculated CH_3 frequencies (both for vacuum and for the condensed phase) are in good agreement with the empirical ones for solid CH_3–$\{F_{11}\}$ (Table S3, ESI†). When R is C_2H_5 and larger, the ionicity of the C–F bond and the hyperconjugated effect in compounds R$\{F_{11}\}$ gradually increase in the series R = C_2H_5, i-C_3H_7, *cyclo*-C_5H_9, and *t*-Bu. Nonetheless, the experiments showed that starting from R = C_2H_5 (and larger), the compounds are purely ionic (Table 7). In the case of the more basic $\{Cl_{11}^-\}$ carborane, an abrupt switch from the covalent to ionic state takes place between $C_2H_5\{Cl_{11}\}$ and i-$C_3H_7^+\{Cl_{11}\}$. For the more basic $CHB_{11}Me_5Br_6^-$

Table 7 The covalent and ionic R–X compounds (X = carborane) identified on the basis of the presence or absence of the strong hyperconjugation effect during R stabilization

Carborane, X	Covalent compounds, R–X	Ionic salts, R^+X^-
$\{F_{11}^-\}$	H_3C–X	R = $C_2H_5^+$ and larger
$\{Cl_{11}^-\}$	H_3C–X, C_2H_5–X	R = i-$C_3H_7^+$ and larger
$CHB_{11}Me_5Br_6^-$ [58]	H_3C–X, C_2H_5–X, i-C_3H_7–X	R = t-$C_4H_9^+$ and larger

carborane, the switch "covalent–ionic state" occurs between i-$C_3H_7\{Cl_{11}\}$ and t-$C_4H_9^+\{Cl_{11}\}$. Thus, the switch from the covalent to ionic state is abrupt, without intermediates. Possibly, this happened because permittivity of carborane compounds is much higher than that of DCE, used in the calculations.

As the calculations revealed, the experimental spectra of carbocations in condensed phases must be compared with those calculated for naked carbocations or carbocations solvated by argon, taking into account that the nature of hyperconjugative stabilization of carbocations does not depend on the phase state. This comparison of cations $C_2H_5^+$, i-Pr^+, and t-Bu^+ is shown in Fig. 7. It uncovered some similarities and some significant discrepancies, already found for t-Bu^+.[28]

The discrepancies can be summarized as follows: (1) the calculated frequencies of hyperconjugated C–H bonds continuously increase as the number of CH_3 groups in carbocations increases ($C_2H_5^+$, i-Pr^+, and t-Bu^+; Fig. 7, red), but this is not the case for the empirically determined dependence (Fig. 7, blue). (2) The calculated frequencies are notably lower than empirical ones for $C_2H_5^+$ and i-Pr^+ and actually coincide only for t-Bu^+, which is mentioned in the literature as proof of a good match between theory and experiment.[1] Judging by the above results, it is obvious that this coincidence is rather accidental. (3) According to calculations, the number of C–H stretches of hyperconjugated CH bonds is equal to the number of CH_3 groups: one for $C_2H_5^+$,

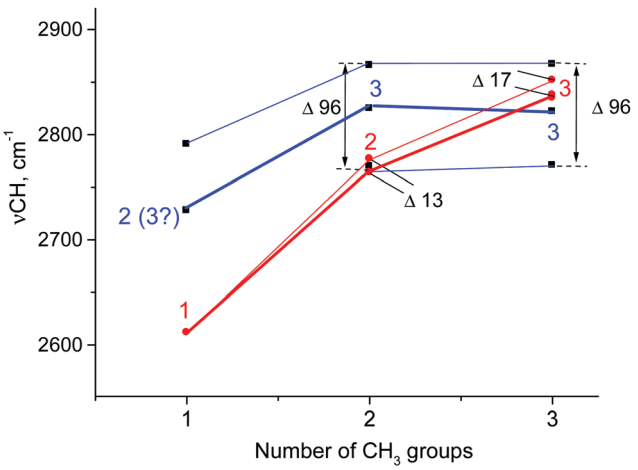

Fig. 7 Dependence of CH stretch frequencies of CH_3 groups involved in hyperconjugation in ethyl$^+$, i-Pr^+, and t-Bu^+ on the number of their CH_3 groups. Empirical data (blue) are shown for $\{F_{11}^-\}$ salts, and the calculated data (red) are shown for cations with a similar type of normal vibrations ($C_2H_5^+$·Ar, C_s; i-Pr^+, C_2; t-Bu+, C_s). The number of CH frequencies is specified. The bold and thin lines represent the most and least intense vibrations, respectively.

two for i-Pr^+, and three for *t*-Bu^+. The experiments imply that these numbers are 2(3), 3 and 3 respectively. (4) The calculated splitting of the bands is rather small (13–17 cm^{-1}) and cannot be detected in the condensed-phase IR spectra because the corresponding bands should be merged into one slightly broadened (degenerated) band. In contrast, experimental spectra show three common bands for CH_3 group vibrations separated by 96 cm^{-1}.

A comparison of the calculated frequencies for the *cyclo*-pentyl$^+$ cation (C_2 symmetry) with the experimental spectrum of *cyclo*-$C_5H_9^+\{F_{11}^-\}$ revealed (Fig. 3) that there is also a significant discrepancy between theory and experiment, as in the case of $C_2H_5^+$ and i-Pr^+ cations. From the experimental spectrum it follows that both CH bonds of the CH_2^{α} group of *cyclo*-pentyl$^+$ are equally influenced by hyperconjugation, and CH_2^{α} and CH_2^{β} are isoelectronic and have the same type of normal vibrations. The same is true for *t*-Bu^+ (and i-Pr_{as}^+): three C–H bonds of CH_3 are equally involved in hyperconjugation, and both CH_3 and CH_3* groups are isoelectronic, with the same type of local group vibrations. Unfortunately, these results contradict computational data.

To try to reconcile the quantum-chemical calculations with the experiment, we performed PBE-D3 computations with periodic boundary conditions for the *t*-Bu$\{Cl_{11}\}$ crystal lattice previously determined by X-ray crystallography.[17] No significant structural changes were found in the fully relaxed unit cell, as compared to the experiment. In contrast, the calculated vibrational frequencies of *t*-Bu^+ in the crystal lattice were found to have the same features as those in gaseous *t*-Bu^+ (Table S5 in ESI†), which again contradict the experimental findings. Similar results follow from the calculations when experimental atomic coordinates were used without relaxation (Table S5 in ESI†). Thus, the origin of inconsistencies in the mechanisms of carbocation hyperconjugation stabilization that follow from calculations and experiments has yet to be established.

Conclusions

According to the experiment, two sets of carbocations exist: with a symmetric and an asymmetric charged core. Our DFT calculations predict no carbocations with an asymmetrical charged core and their results in general contradict the experimental data.

The standard theoretical representation of the mechanism of hyperconjugation predicts that σ-electron density is transferred to the empty $2p_z$ orbital of the sp^2 C atom from one preferred $\mathrm{CH}^{\clubsuit}$ bond of each CH_3 group. At the same time, the σ-electron density on the other CH′ and CH″ bonds slightly increases (Scheme 1). It looks like σ-electrons of the three C–H bonds of the CH_3 group do not merge into molecular orbitals with the generalized electrons. This phenomenon manifests itself in calculated IR spectra, including high-level CCSD(T) computations,[18] as a strong reduction in the $\nu\mathrm{CH}^{\clubsuit}$ frequency (much stronger than in the experiment) making it highly characteristic. Accordingly, vibrations of C–H′ and C–H″ bonds also appear to be highly characteristic ones, which are not mixed with those of the $\mathrm{CH}^{\clubsuit}$ bond. To the best of our knowledge, this case is unknown in the practice of vibrational spectroscopy.

From the experimental data it follows that donation of the σ-electrons from the $\mathrm{CH}^{\clubsuit}$ bond to the empty $2p_z$ orbital of the sp^2 C atom is accompanied by an equal withdrawal of the electron density from C–H′ and C–H″ bonds. That is, the electrons are supplied from each CH bond of the CH_3 group, and the $\mathrm{C–H}^{\clubsuit}$ bond does not act as the predominant donor. Thus, all three bonds of CH_3 groups are equivalent. As a result, the CH stretches manifest themselves as typical CH_3 group vibrations with a smaller red shift (~60–100 cm^{-1}) as compared with that predicted by calculations for $\mathrm{CH}^{\clubsuit}$ stretches (100–200 cm^{-1}). The vibrations of the stronger polarized CH_3* group also appear to be common CH_3 group vibrations with equivalent C–H bonds.

Because calculations revealed that the impact of hyperconjugation on the CH_3 group weakly depends on the dihedral θ angle (the CH_3 rotation around the C–C bond), the donation of the σ-electron density from CH_3 to the empty $2p_z$ orbital of the sp^2 C atom may take place not only *via* the $\mathrm{C–H}^{\clubsuit}$ bond, but also *via* CH′ and CH″ bonds. This mechanism is indicated in Scheme 2 by a dashed arrow.

The aforementioned inconsistencies are valid for all quantum-chemical calculations of naked carbocations known to date. Furthermore, our DFT calculations for the *t*-$Bu^+\{Cl_{11}^-\}$ crystal and R$\{Hal_{11}\}$ molecular compounds in a DCE solution turned out to be comparable with those for naked carbocations, leading to the generally accepted mechanism of hyperconjugative stabilization rather than the mechanism deduced from our experiments.

We can hypothesize that fine electronic structure of carbocations that has not yet been taken into account may be responsible for the observed theory-*versus*-experiment discrepancies. It seems that potential energy surfaces of the carbocations under study are more complicated than expected and cannot be analyzed by the standard quantum-chemical methods such as conventional DFT. This is the subject of our ongoing research.

Undoubtedly, further computational studies in this field, possibly based on the more advanced methods, will result in convergence of the theory with experiment and will allow researchers to explain a number of recently detected features of carbocations, such as the energy equivalence of the CH_3 and CH_3* groups in asymmetric carbocations; why increasing the number of methyl groups from two (i-Pr^+) to three (*t*-Bu^+) does not influence the frequencies of C–H stretches; and the abrupt change in the state of the CH_3* group when *t*-Bu^+ is transferred from gaseous to condensed phases.[28]

Acknowledgements

This work was supported by grant # 16-13-10151 from the Russian Science Foundation and by the Ministry of Education and Science of the Russian Federation within the Project of the joint Laboratories of the Siberian Branch of the Russian Academy of Sciences and National Research Universities. Quantum chemical calculations were supported by the Russian Foundation for Basic Research (grant # 16-03-00357). The Siberian

Supercomputer Center is acknowledged for providing computational resources. The authors thank Irina S. Stoyanova for providing the carborane acids and technical support.

References

1 G. E. Douberly, A. M. Rocks, B. W. Ticknor, P. V. R. Schleyer and M. A. Duncan, *J. Am. Chem. Soc.*, 2007, **129**, 13782.
2 M. A. Dunkan, *J. Phys. Chem. A*, 2012, **116**, 11477.
3 A. M. Ricks, G. E. Douberly, P. V. R. Schleyer and M. A. Dunkan, *Chem. Phys. Lett.*, 2009, **480**, 17.
4 B. Chiavarino, M. E. Crestoni, S. Fornarini, J. Lemaire, L. M. Aleese and P. Maitre, *ChemPhysChem*, 2004, **5**, 1679.
5 G. Olah, E. B. Baker, J. C. Evans, W. S. Tolgyesy, J. S. McIntyre and I. J. Bastien, *J. Am. Chem. Soc.*, 1964, **86**, 1360.
6 H. Vančik, K. Percač and D. E. Sunko, *J. Am. Chem. Soc.*, 1990, **112**, 7418.
7 D. M. Brouwer and E. L. Mackor, *Proc. Chem. Soc.*, 1964, 147.
8 G. A. Olah, *Science*, 1970, **168**, 1298.
9 D. M. Brouwer and H. Hogeveen, *Prog. Phys. Org. Chem.*, 1972, **9**, 179.
10 G. A. Olah, J. M. Bollinger, C. A. Cupas and J. Lukas, *J. Am. Chem. Soc.*, 1967, **89**, 2692.
11 G. A. Olah, J. R. DeMember, A. Commeyras and J. L. Bribes, *J. Am. Chem. Soc.*, 1971, **93**, 459.
12 H. Vančik and D. E. Sunko, *J. Am. Chem. Soc.*, 1989, **111**, 3742.
13 T. Laube, *Acc. Chem. Res.*, 1996, **28**, 399 and references cited therein.
14 T. Kato and C. A. Reed, *Angew. Chem., Int. Ed.*, 2004, **43**, 2908.
15 F. Scholz, D. Himmel, H. Scherer and I. Krossing, *Chem. – Eur. J.*, 2013, **19**, 109.
16 S. Hollenstein and T. Laube, *J. Am. Chem. Soc.*, 1993, **115**, 7240.
17 E. S. Stoyanov, I. V. Stoyanova, F. S. Tham and C. A. Reed, *Angew. Chem., Int. Ed.*, 2012, **51**, 9149.
18 H. Feng, W. Sun, Y. Xie and H. F. Schaefer III, *Chem. – Eur. J.*, 2011, **17**, 10552.
19 S. Sieber, P. Buzek, P. V. R. Schleyer, W. J. Koch and W. de M. Carneiro, *J. Am. Chem. Soc.*, 1993, **115**, 259.
20 G. Rasul, J. L. Chen, G. K. S. Prakash and G. A. Olah, *J. Phys. Chem. A*, 2009, **113**, 6795 and references therein.
21 J. Racine and S. Humbel, *Chem. – Eur. J.*, 2014, **20**, 12601.
22 J. I.-C. Wu and P. von R. Schleyer, *Pure Appl. Chem.*, 2013, **5**, 921.
23 K. B. Wiberg, P. V. R. Schleyer and A. Streitwieser, *Can. J. Chem.*, 1996, **74**, 892.
24 W. Koch, B. Liu and P. V. R. Schleyer, *J. Am. Chem. Soc.*, 1989, **111**, 3479.
25 J. B. Nicholas, T. Xu, D. H. Barich, P. D. Torresa and J. F. Haw, *J. Am. Chem. Soc.*, 1996, **118**, 4202.
26 D. Fărcaşiu and D. Hâncu, *J. Phys. Chem. A*, 1997, **101**, 8695.
27 G. Rasul, J. L. Chen, G. S. Prakash and G. A. Olah, *Comput. Theor. Chem.*, 2011, **964**, 193.
28 E. S. Stoyanov and G. P. Gomes, *J. Phys. Chem. A*, 2015, **119**, 8619.
29 C. Reed, *Chem. Commun.*, 2005, 1669.
30 M. Nava, I. V. Stoyanova, S. Cummings, E. S. Stoyanov and C. A. Reed, *Angew. Chem., Int. Ed.*, 2014, **53**, 1131.
31 M. Juhasz, S. Hoffmann, E. S. Stoyanov, K. Kim and C. A. Reed, *Angew. Chem., Int. Ed.*, 2004, **43**, 5352.
32 E. S. Stoyanov, I. V. Stoyanova, F. S. Tham and C. A. Reed, *J. Am. Chem. Soc.*, 2010, **132**, 4062.
33 E. S. Stoyanov, submitted for publication.
34 A. D. Becke, *J. Chem. Phys.*, 1993, **98**, 5648.
35 C. Lee, W. Yang and R. G. Parr, *Phys. Rev. B: Condens. Matter Mater. Phys.*, 1988, **37**, 785.
36 S. Grimme, J. Antony, S. Ehrlich and H. Krieg, *J. Chem. Phys.*, 2010, **132**, 154104.
37 F. Weigend and R. Ahlrichs, *Phys. Chem. Chem. Phys.*, 2005, **7**, 3297.
38 A. V. Marenich, C. J. Cramer and D. G. Truhlar, *J. Phys. Chem. B*, 2009, **113**, 6378.
39 M. K. Kesharwani, B. Brauer and J. M. L. Martin, *J. Phys. Chem. A*, 2015, **119**, 1701.
40 G. D. Purvis III and R. J. J. Bartlett, *Chem. Phys.*, 1982, **76**, 1910.
41 M. von Hopffgarten and G. Frenking, *Wiley Interdiscip. Rev.: Comput. Mol. Sci.*, 2012, **2**, 43.
42 E. van Lenthe, E.-J. Baerends and J. G. Snijders, *J. Chem. Phys.*, 1993, **99**, 4597.
43 ADF2016, SCM, Theoretical Chemistry, Vrije Universiteit, Amsterdam, The Netherlands, http://www.scm.com.
44 C. F. Guerra, J. G. Snijders, G. te Velde and E. J. Baerends, *Theor. Chem. Acc.*, 1998, **99**, 391.
45 G. te Velde, F. M. Bickelhaupt, E. J. Baerends, C. Fonseca Guerra, S. J. van Gisbergen, J. G. Snijders and T. Ziegler, *J. Comput. Chem.*, 2001, **22**, 931.
46 M. J. Frisch, G. W. Trucks, H. B. Schlegel, G. E. Scuseria, M. A. Robb, J. R. Cheeseman, G. Scalmani, V. Barone, B. Mennucci and G. A. Petersson, *et al.*, *Gaussian 09, Revision D.01*, Gaussian Inc., Wallingford, CT, 2013.
47 J. P. Foster and F. Weinhold, *J. Am. Chem. Soc.*, 1980, **102**, 7211.
48 A. E. Reed, L. A. Curtiss and F. Weinhold, *Chem. Rev.*, 1988, **88**, 899.
49 D. Feller, *J. Comput. Chem.*, 1996, **17**, 1571.
50 K. L. Schuchardt, B. T. Didier, T. Elsethagen, L. Sun, V. Gurumoorthi, J. Chase, J. Li and T. L. Windus, *J. Chem. Inf. Model.*, 2007, **47**, 1045.
51 J. P. Perdew, K. Burke and M. Ernzerhof, *Phys. Rev. Lett.*, 1996, **77**, 3865.
52 G. Kresse and J. Hafner, *Phys. Rev. B: Condens. Matter Mater. Phys.*, 1993, **48**, 13115.
53 G. Kresse and J. Furthmuller, *Phys. Rev. B: Condens. Matter Mater. Phys.*, 1996, **54**, 11169.
54 P. E. Blöchl, *Phys. Rev. B: Condens. Matter Mater. Phys.*, 1994, **50**, 17953.
55 P. Brumer and M. Karplus, *J. Chem. Phys.*, 1973, **58**, 3903.
56 E. S. Stoyanov and S. E. Malykhin, *Phys. Chem. Chem. Phys.*, 2016, **18**, 4871.
57 W. J. Lehmann, C. O. Wilson and I. Shapiro, *J. Chem. Phys.*, 1959, **31**, 1071.
58 T. Kato, E. S. Stoyanov, J. Geier, H. Grutzmacher and C. A. Reed, *J. Am. Chem. Soc.*, 2004, **126**, 12451.